iScience, Volume *25*

Supplemental information

Antibody variable sequences have a pronounced effect on cellular transport and plasma half-life

Algirdas Grevys, Rahel Frick, Simone Mester, Karine Flem-Karlsen, Jeannette Nilsen, Stian Foss, Kine Marita Knudsen Sand, Thomas Emrich, Jens Andre Alexander Fischer, Victor Greiff, Inger Sandlie, Tilman Schlothauer, and Jan Terje Andersen

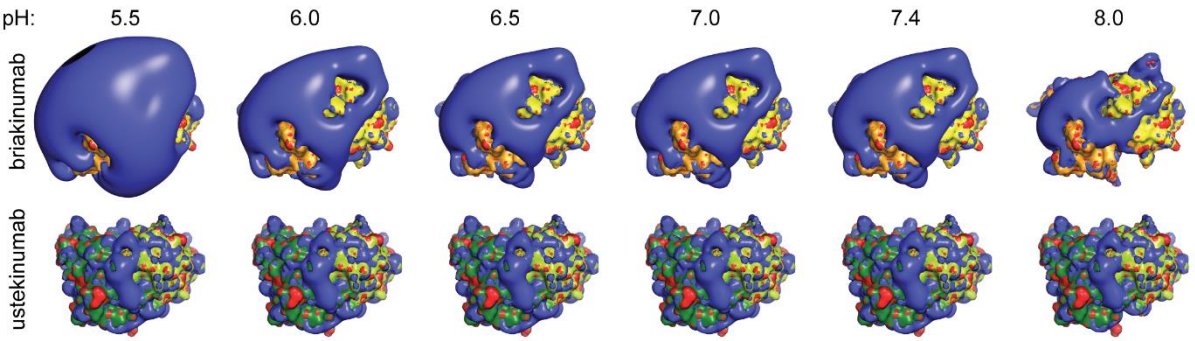

Figure S1. Changes in charge distribution of top oriented ustekinumab and briakinumab Fv through a pH range from 5.0 to 9.0, related to Figure 1. The HCs of ustekinumab and briakinumab are shown in green and orange, and the LCs of ustekinumab and briakinumab are coloured in light green and yellow, respectively. The blue colour indicates positive charge, the red – negative charge.

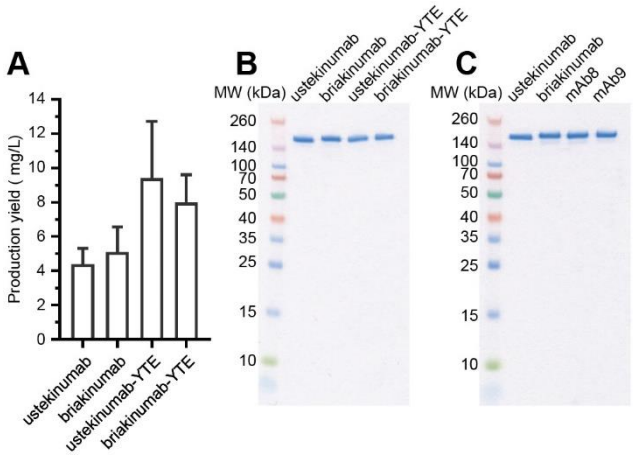

Figure S2. Production and integrity of ustekinumab and briakinumab variants, related to Figure 2. (**A**) An average yield of recombinant ustekinumab and briakinumab variants produced from transient transfection of HEK293E cells. Data are presented as mean ± s.d. From three independent production of IgG variants. (**B** and **C**) Non-reducing SDS-PAGE analysis of ustekinumab and briakinumab variants.

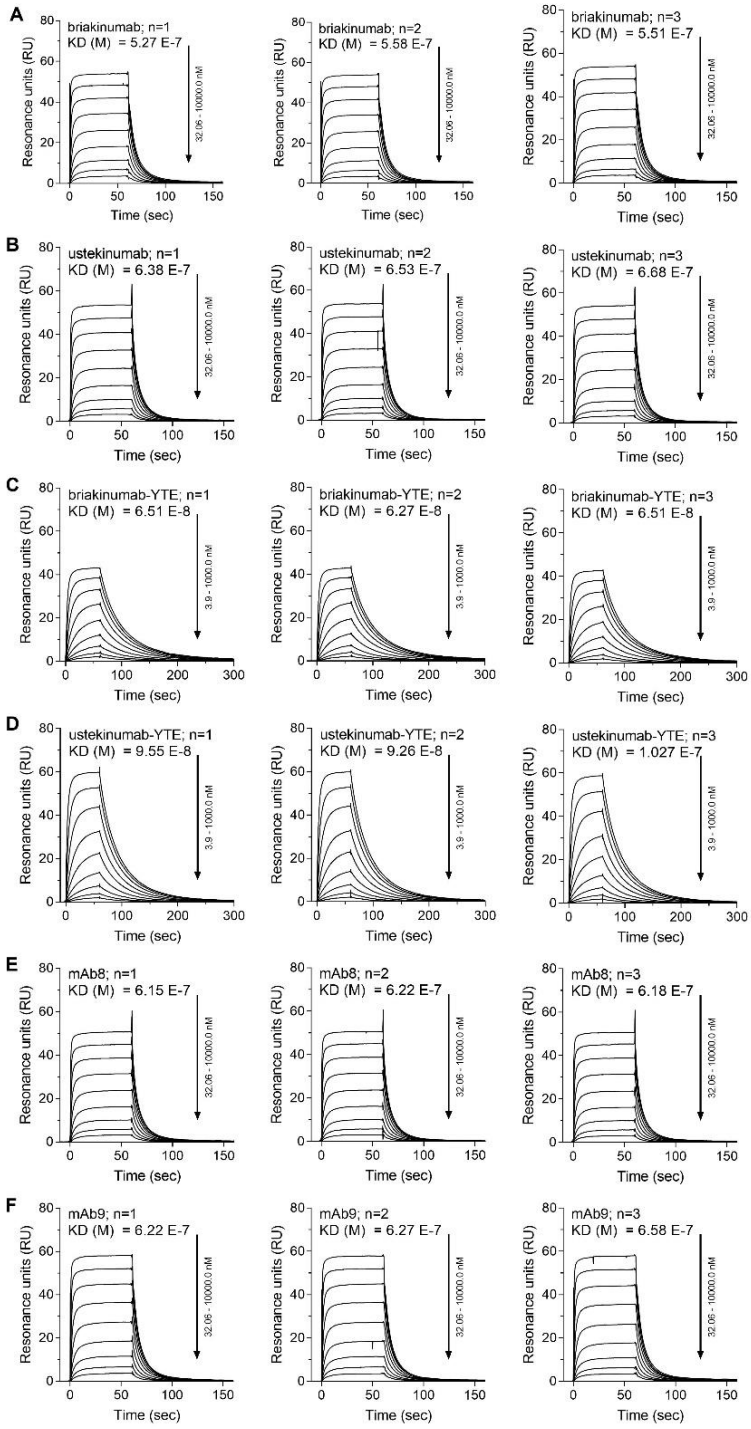

Figure S3. SPR measurement of IgG binding to hFcRn, related to Figure 2. Representative sensorgrams showing binding of titrated amounts of monomeric hFcRn injected over immobilized (100 RU) (**A**) briakinumab, (**B**), ustekinumab (**C**), briakinumab-YTE (**D**), ustekinumab-YTE (**E**) mAb8 and (**F**) mAb9 at pH 5.5. The obtained sensorgrams were fitted to the Langmuir 1:1 binding model. Injections were performed with a flow rate of 30 µl/min at 25 °C. n is indicating an individual experiment.

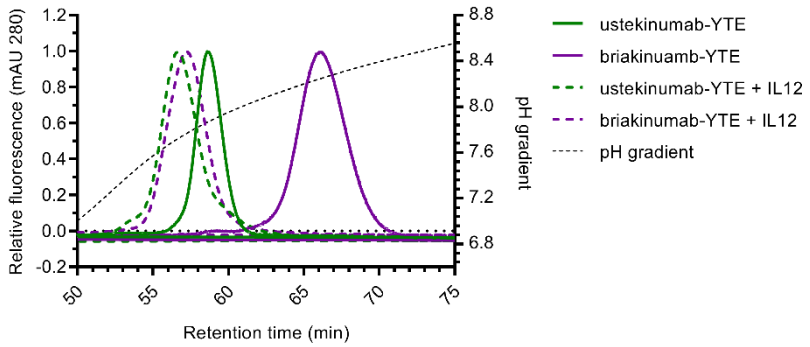

Figure S4. Analytical hFcRn affinity chromatography, related to Figure 2. Ustekinumab-YTE and briakinumab-YTE were applied as monomeric fractions and in complex with IL-12. The elution profiles are shown as relative fluorescence intensity and a function of the pH gradient. Fluorescence intensity was normalised and set to one for the clarity. Data are shown as one representative experiment out of three.

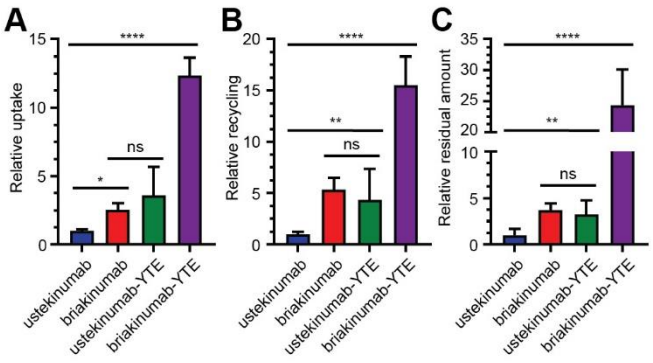

Figure S5. HERA screening of ustekinumab, briakinumab and their respective YTE mutants, related to Figure 4. (**A**) Relative uptake of WT and Fc-engineered hIgG$_1$ variants when 400 nM of each variant was added to the cells followed by 4 h incubation, washing and lysis of the cells. (**B**) Relative recycling of the Fc-engineered hIgG$_1$ variants when 400 nM of each variant was added to the cells and incubated for 4 h followed by extensive washing and additional overnight incubation before sample collection. (**C**) Relative residual amount of WT and Fc-engineered hIgG$_1$ variants. The same procedure as in (**B**) followed by lysis of the cells. The amounts of IgG$_1$ variants in all samples were quantified by ELISA and obtained data are shown as mean ± s.d. of three independent experiments performed in (a-d) triplicates. ns - not significant, *p < 0.05, **p < 0.01, ***p < 0.001 and ****p < 0.0001, by one-way ANOVA (Turley's multiple comparison test).

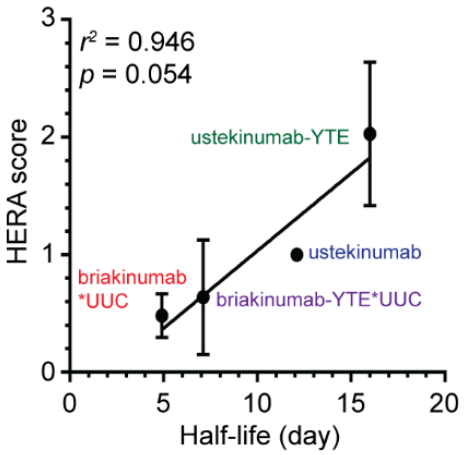

Figure S6. Correlation of the derived HERA scores with plasma half-life values obtained from hFcRn transgenic mice, related to Figure 4. Data from Figure 4 was used to calculate correlation between HERA score and half-life values. Data is represented as mean ± s.d.

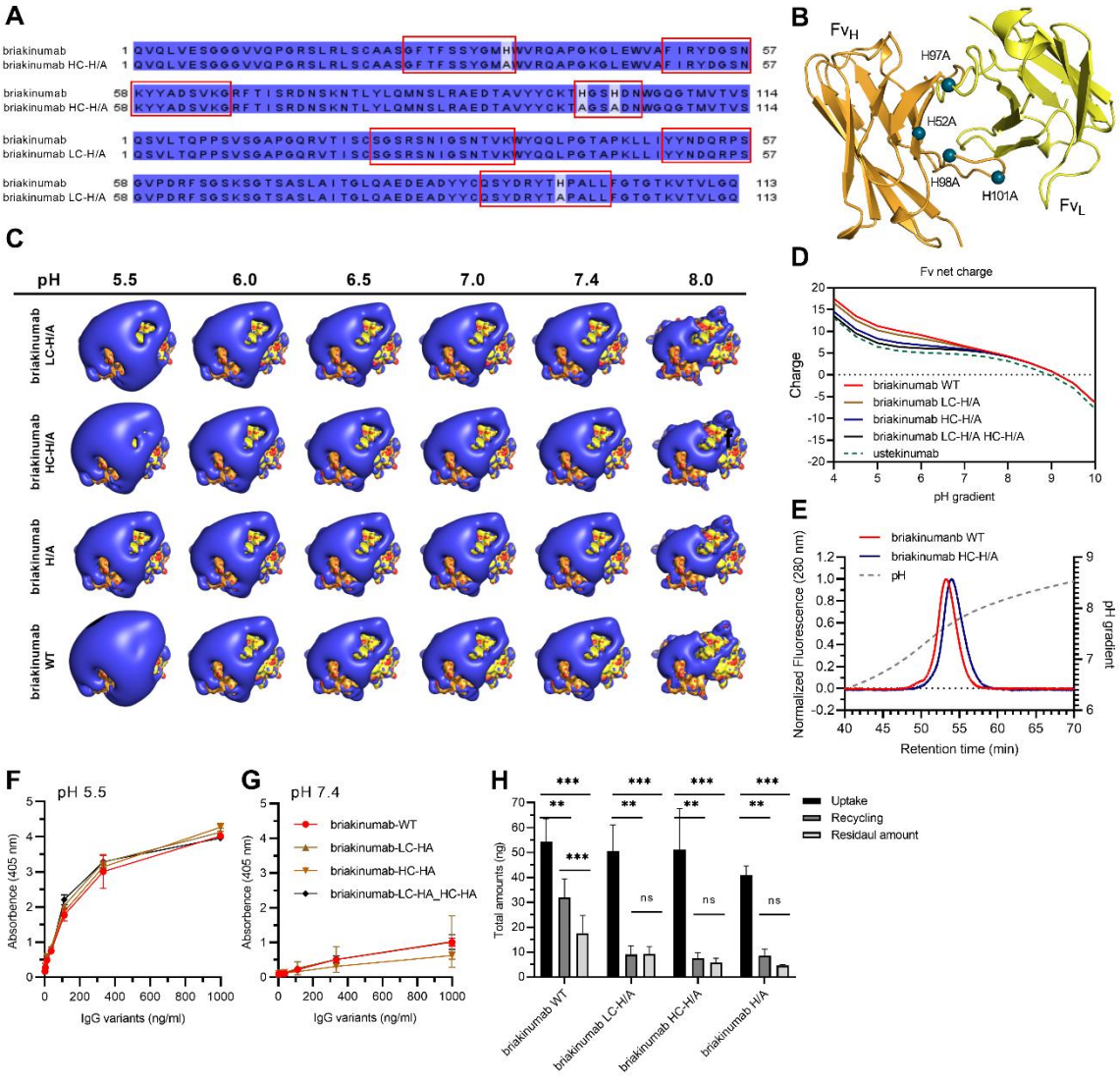

Figure S7. Fv-engineering of briakinumab modulates binding to FcRn and cellular uptake, related to Figure 5. (**A**) Sequence alignments of HC and LC of briakinumab and CDR mutations. Conserved and non-conserved amino acid residues are marked in dark and light blue, respectively, while CDR sequences are highlighted by red squares. Sequence alignments have been made by Jalview. (**B**) Crystal structure of top orientated briakinumab Fv showing the histidine residues that were substituted to alanine residues. The HC of briakinumab are shown in orange, and the LC of are coloured in yellow, respectively. (**C**) The charge distribution of top oriented Fv of briakinumab LC-H/A, briakinumab HC-H/A, briakinumab H/A and briakinumab WT throughout the pH gradient from 5.5 to 8.0.The blue and red colours indicate positive and negative charges, respectively. (**D**) Sequence-based calculation of net charge through pH range of Fv of briakinumab, briakinumab LC-H/A, briakinumab HC-H/A and briakinumab H/A. Sequence alignments have been made by Jalview. The figures were designed using PyMOL (www.pymol.org) with the crystallography data of human IgG1 and net charges

were calculated with Emboss iep (www.bioinformatics.nl). (**E**) Analytical hFcRn affinity chromatography of briakinumab WT and briakinumab HC-H/A as monomeric fractions. The elution profiles are shown as relative fluorescence intensity and as a function of pH gradient. Fluorescence intensity was normalised and set to one for the clarity. Data are shown as one representative experiment out of three. (**F**-**G**) ELISA binding of titrated amounts (0.5-1,000.0 ng/ml) of, briakinumab WT, briakinumab LC-H/A, briakinumab HC-H/A and briakinumab H/A to hFcRn at pH (**f**) 5.5 and (**G**) 7.4. Data are mean ± s.d. of one representative experiment out of three. (**H**) HERA results of briakinumab WT, briakinumab LC-H/A, briakinumab HC-H/A and briakinumab H/A when 400 nM of each variant was added to the cells followed by 3 h incubation, washing and lysis of the cells. In addition, recycling sample of variants were collected when 400 nM of each variant was added to the cells and incubated for 3 h followed by extensive washing and additional 3 h incubation before sample collection. Further, cells were washed and lysed to measure the residual amount of briakinumab variants. The amounts of IgG_1 variants in all samples were quantified by ELISA and obtained data are shown as mean ± s.d of one representative experiment performed in triplicates out of two independent experiments. HERA data has been analysed by Two-away Anova (Tukey's multiple comparison test, $^{**}p = 0.0023$, $^{***}p < 0.0001$, ns – not significant).

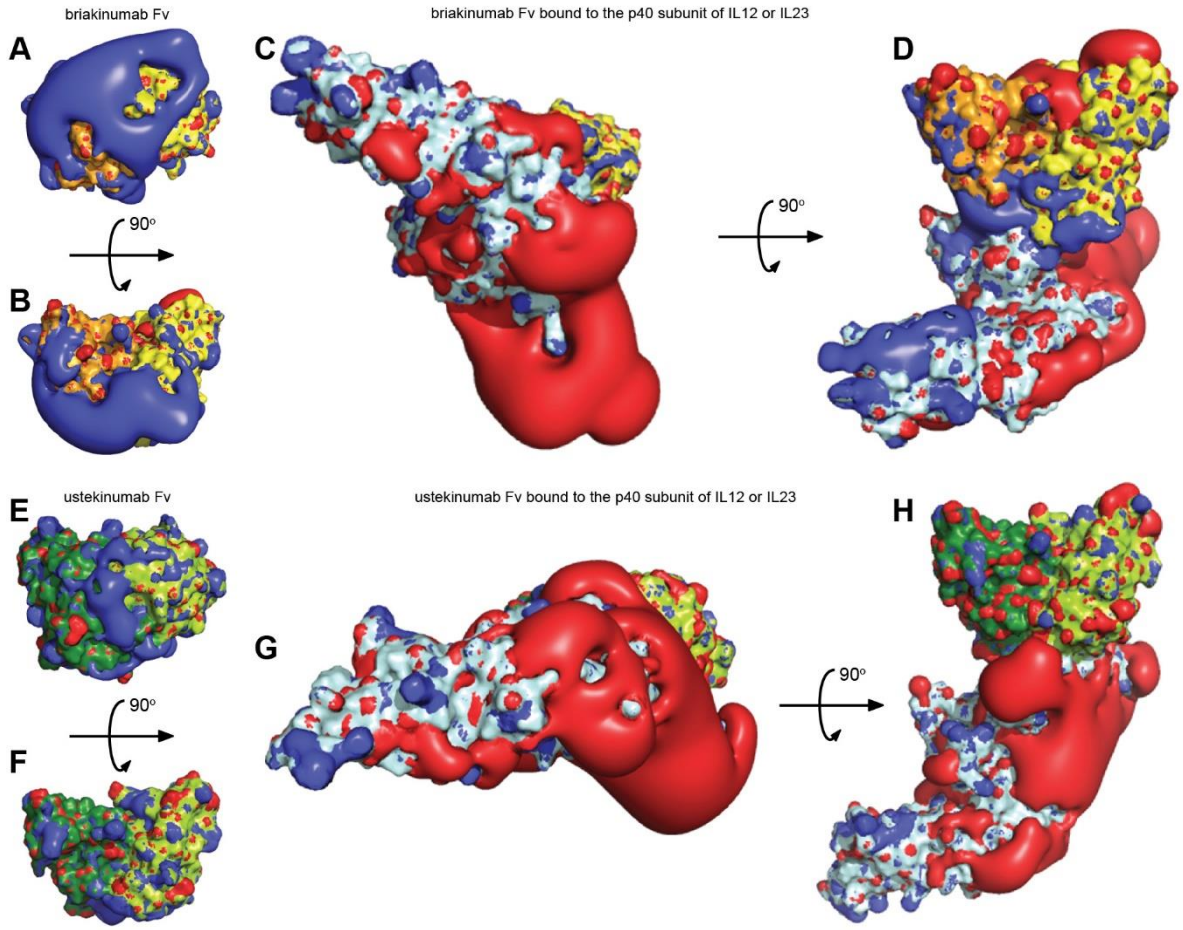

Figure S8. Charge distribution of ustekinumab and briakinumab Fv alone and in complex with the p40 subunit of IL12 or IL23, related to Figure 5. The charge distribution of top oriented (**A**) and (**B**) rotated 90̊ around x-axis briakinumab Fv alone or (**C** and **D**) in complex with p40 subunit of IL-12 or IL-23 at two different orientation. The charge distribution of top oriented (**E**) and (**F**) rotated 90̊ around x-axis ustekinumab Fv alone or (**G** and **H**) in complex with p40 subunit of IL12 or IL23 at two different orientations. Charge distribution was calculated at pH 7.4. The crystal structures of ustekinumab Fab (3HMW), briakinumab Fab (5N2K), ustekinuman-IL-12 complex (3HMX) and brakinnumab-IL23 complex (5NJD) have been used to calculate charge distribution. The p40 subunit of IL-12 and IL-23 was used without p35 and p19 subunits for clarity, respectively. Blue colour indicates positive charge, red – negative charge. The HCs of ustekinumab and briakinumab are shown in green and orange, and the LCs of ustekinumab and briakinumab are coloured in light green and yellow, while p40 subunit of IL-12 or IL-23 is shown in light grey, respectively.

Table S1. Protein sequences of ustekinumab and briakinumab Fv domains were used for net charge calculation, related to Figure 1 and 5. CDR loops of both antibodies were defined by Rosetta. Antibodies framework sequences are a variable domain sequence without CDRs.

CDRs	ustekinumab	briakinumab
H1	GYSFTTYWLG	GFTFSSYGMH
H2	IMSPVDSDIRYSPSFQG	FIRYDGSNKYYADSVKG
H3	RRPGQGYFDF	HGSHDN
L1	RASQGISSWLA	SGSRSNIGSNTVK
L2	AASSLQS	YNDQRPS
L3	QQYNIYPYT	QSYDRYTHPALL
framework HC	EVQLVQSGAEVKKPGESLKISCKGSWVR QMPGKGLDWIGQVTMSVDKSITTAYLQ WNSLKASDTAMYYCARWGQGTLVTVS	QVQLVESGGGVVQPGRSLRLSCAASWV RQAPGKGLEWVARFTISRDNSKNTLYLQ MNSLRAEDTAVYYCKTWGQGTMVTVS
framework κ LC	DIQMTQSPSSLSASVGDRVTITCWYQQK PEKAPKSLIYGVPSRFSGSGSGTDFTLTIS SLQPEDFATYYCFGQGTKLEIKR	QSVLTQPPSVSGAPGQRVTISCWYQQLP GTAPKLLIYGVPDRFSGSKSGTSASLAIT GLQAEDEADYYCFGTGTKVTVLGQ

Table S2. Binding kinetics derived from SPR analysis, related to Figure 2 and Figure S3.

$hIgG_1$ variants[a]	k_a (10^5 M^{-1} s^{-1})	k_d (10^{-2} s^{-1})	K_D[b] (nM)	Chi^2[c]
ustekinumab	2.0 ± 0.1	13.3 ± 0.2	653.0	0.4
briakinumab	2.0 ± 0.1	10.9 ± 0.1	545.2	0.7
ustekinumab-YTE	2.7 ± 0.3	0.3 ± 0.0	95.5	0.2
briakinumab-YTE	3.3 ± 0.1	0.2 ± 0.0	64.0	0.2
mAb8	2.1 ± 0.0	12.9 ± 0.1	616.9	0.4
mAb9	1.9 ± 0.1	12.1 ± 0.1	636.2	0.6

[a,] The $hIgG_1$ variants were immobilized on CM5 Series S sensor chips (~100 RU) and two-fold serial dilutions of his-tagged hFcRn were injected at pH 5.5.

[b,] The kinetic rate constants were obtained using a Langmuir 1:1 bimolecular binding model. The kinetic values represent the mean ± s.d. of triplicates.

[c,] Chi^2 is a measure of the average squared residual.

Supplementary Table S3. Analytical hFcRn affinity chromatography analysis, related to Figures 2M-N and Figure S4.

hIgG1 variants	Retention time (min)			pH value		
	start of peak	top of peak	end of peak	start of peak	top of peak	end of peak
ustekinumab	50.7	52.4	54.1	7.0	7.2	7.4
briakinumab	53.78	56.8	60.2	7.40	7.7	8.0
mAb8	54.95	57.1	59.14	7.4	7.6	7.7
mAb9	53.27	54.7	56.05	7.2	7.4	7.5
ustekinumab-YTE	57.1	59.3	61.7	7.7	7.9	8.1
briakinumab-YTE	64.1	68.9	73.8	8.2	8.4	8.5
ustekinumab + IL12	48.7	52.3	56.6	6.8	7.1	7.5
briakinumab + IL12	48.4	51.4	55.0	6.7	7.0	7.4
ustekinumab + IL12	54.3	56.6	60.1	7.3	7.5	7.8
briakinumab + IL12	54.7	57.2	59.9	7.3	7.6	7.8
YTE/KF*	72.6	77.6	83.0	8.5	8.6	8.7
KF*	51.8	56.7	61.4	7.8	8.0	8.2

*YTE/KF and KF are hIgG1 variants with the NIP specificity. The retention time and pH values of dissociation of IgG1 variants from the hFcRn column have been published by Grevys et, at. Nat. Comm., 2018.